



Cite this: DOI: 10.1039/c5tc03919c

## Eu<sup>3+</sup> ion concentration induced 3D luminescence properties of novel red-emitting Ba<sub>4</sub>La<sub>6</sub>(SiO<sub>4</sub>)O:Eu<sup>3+</sup> oxyapatite phosphors for versatile applications

G. Seeta Rama Raju,<sup>a</sup> E. Pavitra,<sup>a</sup> Sk. Khaja Hussain,<sup>a</sup> D. Balaji,<sup>b</sup> and Jae Su Yu<sup>a\*</sup>

A series of Eu<sup>3+</sup> ions activated Ba<sub>4</sub>La<sub>6</sub>(SiO<sub>4</sub>)<sub>6</sub>O (BLSO:Eu<sup>3+</sup>) phosphors were synthesized by a modified citrate sol-gel process. The structural properties of these phosphors were explored by means of X-ray diffraction (XRD) and Fourier transform infrared spectroscopy. The XRD patterns confirmed their oxyapatite structure with the space group of  $P6_3/m$  after annealing at 1400 °C. The scanning electron microscope image exhibited the irregular morphology of BLSO:Eu<sup>3+</sup> particles and the elemental mapping confirmed that the Eu<sup>3+</sup> ions were distributed homogeneously on the La<sup>3+</sup> ion sites. Photoluminescence (PL) excitation spectra of BLSO:Eu<sup>3+</sup> exhibited the charge transfer band (CTB) and intense f-f transitions of Eu<sup>3+</sup> ions in the violet and blue wavelength regions. The CTB intensity decreased and the f-f transition of Eu<sup>3+</sup> ions increased with increasing the Eu<sup>3+</sup> ion concentration due to the presence of defects in the 4f and 6h sites of the BLSO host lattice. This feature facilitates the strong absorption in the near-ultraviolet (NUV) region, which is useful for high color rendering index NUV based white light-emitting diodes for display and lighting applications. The PL spectra displayed intense red emission ( $^5D_0 \rightarrow ^7F_2$ ) along with considerable orange emission ( $^5D_0 \rightarrow ^7F_1$ ) with good asymmetry ratios and chromaticity coordinates, and exhibited better emission performance than that of commercial Y<sub>2</sub>O<sub>3</sub>:Eu<sup>3+</sup> phosphors. The three-dimensional PL spectra revealed their strong emission characteristics under UV, NUV and visible excitation wavelengths. The cathodoluminescence properties were also similar to the PL results, confirming that the BLSO:Eu<sup>3+</sup> phosphors emit stable red emission under different excitation sources as compared to the commercial Y<sub>2</sub>O<sub>3</sub>:Eu<sup>3+</sup> phosphors.

Received 23rd November 2015,  
Accepted 31st December 2015

DOI: 10.1039/c5tc03919c

www.rsc.org/MaterialsC

## Introduction

In recent years, solid-state lighting (SSL) related light-emitting diodes (LEDs) have been developed based on different excitation sources from ultraviolet (UV) to infrared regions, and their use has been extended from exterior to interior lighting and display applications.<sup>1–4</sup> Compared with traditional incandescent and fluorescent lamps, white LEDs (WLEDs) have significant potential for a wide range of illumination applications owing to their better advantages such as high efficiency, long working lifetime, durability, low power consumption, and environmental compassion due to the non-usage of mercury.<sup>5–10</sup> To date, currently available WLEDs on the market are mostly blue-emitting GaN chips (450–460 nm) combined with yellow-emitting Y<sub>3</sub>Al<sub>5</sub>O<sub>12</sub>:Ce<sup>3+</sup> (YAG:Ce<sup>3+</sup>) phosphors. However, these WLEDs suffer from a poor color-rendering index (CRI) as well as

thermal quenching at elevated temperatures.<sup>9–12</sup> To overcome these shortcomings, nowadays, the WLEDs fabricated using near-UV (NUV) LED chips have attracted much attention because they provide a higher excitation efficiency than those using blue chips.<sup>2,10,13–18</sup> Therefore, the demand for novel phosphors with an excitation band in the NUV spectral region has been rapidly increasing.<sup>19</sup>

Among different monochromatic phosphors, red color-emitting phosphors play an important role in the SSL applications not only to increase the CRI of WLEDs but also for use in the plant cultivation.<sup>20</sup> Usually, plants grow better under red LEDs compared to that of daylight fluorescent lamps since the red light is close to the maximum absorbance for chlorophyll.<sup>20–22</sup> In this context, our search has continued on the development of a physically and chemically stable red color-emitting novel oxide phosphor with considerable absorption from UV to visible ranges.

It is well known that the silicates have different kinds of crystal structures and serve as a good luminescent material.<sup>8,23–26</sup> Among the several crystal structures of silicates, oxyapatite structured materials with the space group of  $P6_3/m$  exhibit excellent thermal and chemical stabilities.<sup>26–30</sup> In the literature, a variety of silicate based oxyapatite luminescent materials have

<sup>a</sup> Department of Electronics and Radio Engineering, Institute for Wearable Convergence Electronics, Kyung Hee University, 1 Seocheon-dong, Gicheung-gu, Yongin-si, Gyeonggi-do 446-701, Republic of Korea. E-mail: jsyu@khu.ac.kr; Fax: +82-31-206-2820; Tel: +82-31-201-3820  
<sup>b</sup> Crystal Growth Centre, Anna University, Chennai- 600025, India

been reported. For example, Eu<sup>3+</sup> ions doped Ca<sub>4</sub>Y<sub>6</sub>(SiO<sub>4</sub>)<sub>6</sub>O,<sup>31</sup> Ba<sub>2</sub>Gd<sub>8</sub>(SiO<sub>4</sub>)<sub>6</sub>O<sub>2</sub>,<sup>32</sup> Sr<sub>2</sub>Y<sub>8</sub>(SiO<sub>4</sub>)<sub>6</sub>O<sub>2</sub>,<sup>33,34</sup> and Ca<sub>2</sub>Gd<sub>8</sub>(SiO<sub>4</sub>)<sub>6</sub><sup>35</sup> host lattices showed efficient red emissions under UV and NUV excitation wavelengths. However, all the excitation peak intensities increased with increasing the annealing temperature or concentration of Eu<sup>3+</sup> ions. In contrast to the reported silicate based oxyapatite structures, we found that the defect oxyapatite of the novel Ba<sub>4</sub>La<sub>6</sub>(SiO<sub>4</sub>)O host lattice exhibited favorable luminescence properties when doped with Eu<sup>3+</sup> ions.

Although the Ba<sub>4</sub>La<sub>6</sub>(SiO<sub>4</sub>)<sub>6</sub>O defect oxyapatite host lattice was first reported by J. W. ter Vrugt *et al.* (based on JCPDS card no. 27-0037), no reports have been found on the luminescence properties of this host lattice so far. Therefore, for the first time, we report on the Eu<sup>3+</sup> ions doped Ba<sub>4</sub>La<sub>6</sub>(SiO<sub>4</sub>)<sub>6</sub>O host lattice (hereafter referred to as BLSO:Eu<sup>3+</sup>) by a sol-gel process. This phosphor exhibited the Eu<sup>3+</sup> ion concentration induced photoluminescence (PL) excitation (PLE) along with good PL properties when exciting in different excitation regions. The PL properties were explained by means of three-dimensional (3D) emission spectra and the cathodoluminescence (CL) properties were evaluated under electron beam excitations. The obtained results suggested that the BLSO:Eu<sup>3+</sup> phosphors are a promising novel red-emitting material under different excitation sources for various applications.

## Experimental

BLSO:Eu<sup>3+</sup> phosphors with the composition of Ba<sub>4</sub>La<sub>6(1-x)</sub>(SiO<sub>4</sub>)<sub>6</sub>O:6xEu<sup>3+</sup> were synthesized by a modified citrate sol-gel process. Stoichiometric amounts of barium nitrate [Ba(NO<sub>3</sub>)<sub>2</sub> ( $\geq 99\%$ )], lanthanum nitrate hexahydrate [La(NO<sub>3</sub>)<sub>3</sub>·6H<sub>2</sub>O ( $99.99\%$ )], europium nitrate pentahydrate [Eu(NO<sub>3</sub>)<sub>3</sub>·5H<sub>2</sub>O ( $99.9\%$ )], tetraethyl orthosilicate (TEOS) [Si(O<sub>2</sub>C<sub>2</sub>H<sub>5</sub>)<sub>4</sub> ( $98\%$ )], and citric acid [HOC(COOH)(CH<sub>2</sub>COOH)<sub>2</sub>·( $\geq 99.5\%$ )] were used. At first, solution I was prepared by dissolving 4 mM of barium nitrate, 6(1 - x) mM of lanthanum nitrate, and 6x mM of europium nitrate in 180 ml of de-ionized (DI) water. Solution II was prepared by dissolving an appropriate amount of TEOS in 20 ml of 2-PrOH. The required amount of (32 mM) citric acid was added to the solution I (metal ions and citric acid ratio of 1 : 2) and both the solutions were stirred using a magnetic stirrer until the homogeneous solutions were formed. After that, the solutions I and II were mixed and the magnetic stirring was continued until the formation of homogeneous solution. Then, the mixed solution was heated on a hot plate and the solution temperature was maintained at 80 °C. To obtain a homogeneous heating throughout the solution, the beaker was wrapped with a polythene cap under the continued magnetic stirring for 1 h and then the cap was removed. The solution was evaporated slowly until the yellowish wet gel was formed. The obtained sol-gel was then dried in an oven at 120 °C for a day. After drying the sol-gel, a porous solid matrix so-called xerogel was formed. The xerogel was decomposed upon further heating at 500 °C for 4 h, thus producing black-colored flakes with highly fine particles. The resulting powders were further annealed at different temperatures for 12 h.

The X-ray diffraction (XRD) patterns of the BLSO:Eu<sup>3+</sup> phosphors were recorded on a Mac Science (M18XHF-SRA) X-ray powder diffractometer with CuK $\alpha$  = 1.5406 Å. The morphological feature and the energy dispersive X-ray spectroscopy (EDS) spectrum were observed by the high-resolution field-emission scanning electron microscope (HR FE-SEM:CARL ZEISS, MERLIN) image. Fourier transform infrared (FTIR) spectrum of the BLSO:Eu<sup>3+</sup> phosphors was recorded on a thermo Nicolet-5700 spectrophotometer. The room-temperature PL and 3D PL spectra were measured by using a Scineco Fluromate FS-2 and the lifetime measurement was performed by using a Photon Technology International (PTI, USA) fluorimeter with the attachment of a Xe-flash lamp of 25 W power. The temperature dependent PL measurements were carried out using the FLS920 fluorescence spectrophotometer equipped with a 450 W Xe lamp as the excitation source. The quantum yield (or internal quantum efficiency) and absorption efficiency measurements were carried out using a fluorescence spectrophotometer equipped with the integrating sphere (Hamamatsu Photonics C9920-02). The CL properties were measured using a Gatan (UK) MonoCL3 system attached with the SEM (Hitachi S-4300 SE).

## Results and discussion

Fig. 1 shows the XRD patterns of 6 mol% Eu<sup>3+</sup> ions doped BLSO (BLSO:6Eu<sup>3+</sup>) phosphors annealed at the temperatures of 1300 and 1400 °C for 12 h. After annealing at 1300 °C, the BLSO:6Eu<sup>3+</sup> phosphor exhibited some impurity peaks of La<sub>2</sub>Si<sub>2</sub>O<sub>7</sub> (JCPDS No. 48-0052) at the lower angle side. However, after annealing at 1400 °C, all of the diffraction peaks were well indexed to the oxyapatite hexagonal structure according to the standard JCPDS No. 27-0037 and space group P6<sub>3</sub>/m (176). The crystallite sizes from the XRD patterns were calculated by the well-known Scherrer equation:

$$D_{hkl} = \frac{K\lambda}{\beta \cos \theta} \quad (1)$$

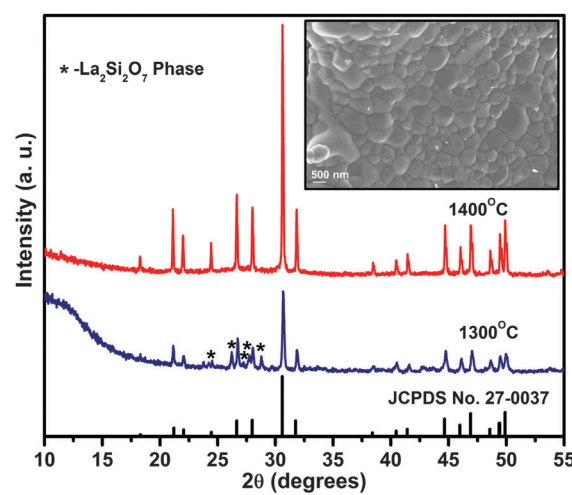


Fig. 1 XRD patterns of the BLSO:6Eu<sup>3+</sup> phosphor at different annealing temperatures (the inset shows the SEM image of the BLSO:6Eu<sup>3+</sup> phosphor).

where  $D$  is the average crystallite size,  $\lambda$  is the X-ray wavelength (1.5406 Å),  $k$  is the shape factor (0.9),  $\beta$  is the full width at half maximum (FWHM), and  $\theta$  is the diffraction angle of an observed peak, which yielded an average crystallite size of 99.4 nm. To further confirm that the Eu<sup>3+</sup> ions doped BLSO formed in the oxyapatite phase, Rietveld refinement was performed on the XRD pattern using the software General Structure Analysis System (GSAS). Fig. 2a presents the Rietveld refinement results for the BLSO:6Eu<sup>3+</sup> phosphor, and its crystallographic data are summarized in Table 1. The observed and calculated results are near to those reported in the literature under JCPDS card no. 27-0037, in which the BLSO host lattice adopted an oxyapatite structure with space group  $P6_3/m$  (176). However, from the BLSO and BLSO:6Eu<sup>3+</sup> lattice parameters, it was recognized that the structure faintly contracted along  $a$ ,  $b$ , and  $c$  axes as the Eu<sup>3+</sup> ions doped into the La<sup>3+</sup> sites. This shrinkage of BLSO:6Eu<sup>3+</sup> lattice parameters is due to the slight difference in the ionic radius between La<sup>3+</sup> ( $r_{\text{VII}} = 1.1$  Å,  $r_{\text{IX}} = 1.216$  Å) and Eu<sup>3+</sup> ( $r_{\text{VII}} = 1.01$  Å,  $r_{\text{IX}} = 1.12$  Å) ions. Using Diamond software, the ideal unit cell was modeled based on the acquired atomic coordinates, as shown in Fig. 2(b). In this oxyapatite structure, Ba<sub>1</sub><sup>2+</sup>/La<sub>1</sub><sup>3+</sup>/Eu<sub>1</sub><sup>3+</sup> ions occupy the nine-fold coordinated 4f site (Fig. 2c) and Ba<sub>1</sub><sup>2+</sup>/La<sub>1</sub><sup>3+</sup>/Eu<sub>1</sub><sup>3+</sup> ions occupy the seven-fold coordinated 6h site (Fig. 2d), which are connected with the isolated SiO<sub>4</sub> tetrahedra. Based on the Rietveld refinement, the site occupancy factor comparison between BLSO and BLSO:6Eu<sup>3+</sup> phosphors are presented in Table 1. The inset of

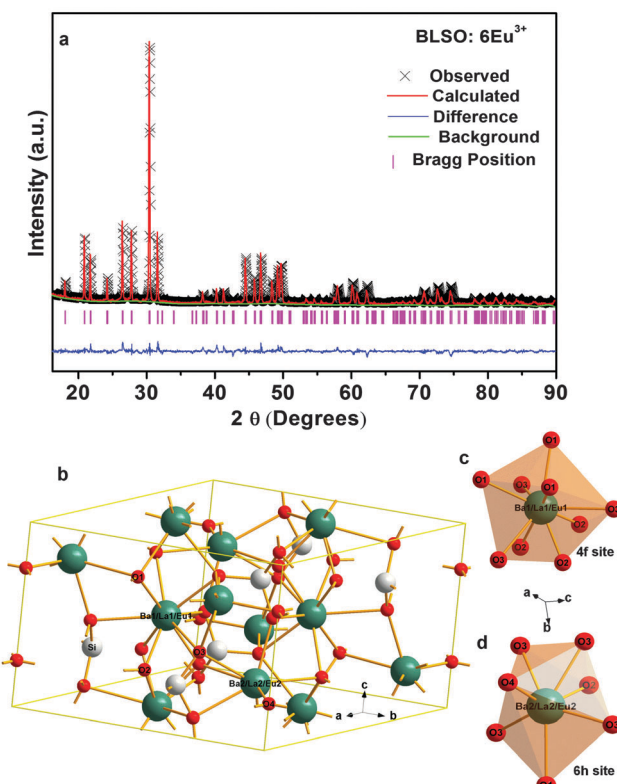


Fig. 2 (a) Rietveld refinement and (b) ideal unit cell crystal structure of the BLSO:6Eu<sup>3+</sup> phosphor. (c) 4f site occupation of 9-fold coordinated and (d) 6h site occupation of 7-fold coordinated Ba<sup>2+</sup>/La<sup>3+</sup>/Eu<sup>3+</sup> ions.

Table 1 Crystallographic data with atomic and lattice parameters of the BLSO:6Eu<sup>3+</sup> phosphor

| Atom | Wyckoff position | Atomic coordinates of BLSO:6Eu <sup>3+</sup> |          |          | Site occupancy factor |                        |
|------|------------------|--|----------|----------|-----------------------|------------------------|
|      |                  | x  | y        | z        | BLSO                  | BLSO:6Eu <sup>3+</sup> |
| Ba1  | 4f               | 1/3  | 2/3      | -0.00475 | 0.06                  | 0.30457                |
| La1  | 4f               | 1/3  | 2/3      | -0.00475 | 0.7902                | 0.66487                |
| Eu1  | 4f               | 1/3  | 2/3      | -0.00475 | 0.035                 |                        |
| Ba2  | 6h               | 0.23255                                      | -0.01411 | 1/4      | 0.6921                | 0.54671                |
| La2  | 6h               | 0.23255                                      | -0.01411 | 1/4      | 0.3012                | 0.38575                |
| Eu2  | 6h               | 0.23255                                      | -0.01411 | 1/4      |                       | 0.03763                |
| Si   | 6h               | 0.39807                                      | 0.35834  | 1/4      | 1                     | 1                      |
| O1   | 6h               | 0.34200                                      | 0.48300  | 1/4      | 1                     | 1                      |
| O2   | 6h               | 0.61784                                      | 0.44594  | 1/4      | 0.3721                | 0.36272                |
| O3   | 12i              | 0.35186                                      | 0.26347  | 0.07214  | 0.5528                | 0.53853                |
| O4   | 2a               | 0  | 0        | 1/4      | 0.5691                | 0.56592                |

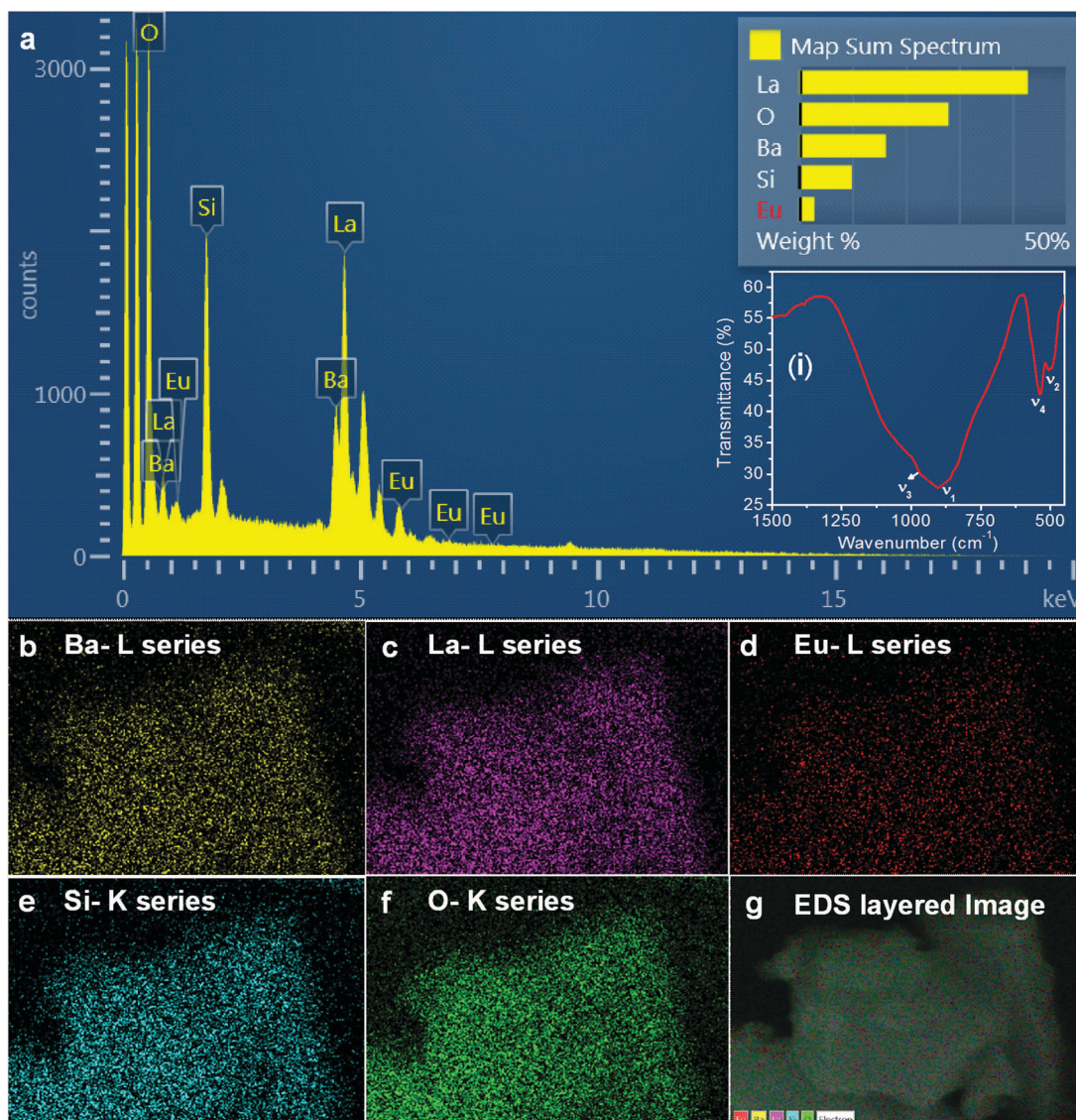
**Rietveld data**  
Program GSAS  
Structure Hexagonal  
Space group  $P6_3/m$   
BLSO  $\Rightarrow a = 9.7791$  Å,  $c = 7.3194$  Å,  $V = a^2 c \sin(60^\circ) = 606.18$  Å<sup>3</sup>  
BLSO:6Eu<sup>3+</sup>  $\Rightarrow a = 9.7749$  Å,  $c = 7.3108$  Å,  $V = a^2 c \sin(60^\circ) = 604.95$  Å<sup>3</sup>  
 $R_p = 6.04\%$ ,  $R_{wp} = 9.05\%$ ,  $RF^2 = 9.4\%$ ,  $\chi^2 = 1.545$

Fig. 1 shows the HR FE-SEM image of the BLSO:6Eu<sup>3+</sup> phosphor, indicating the irregular morphology with irregular sizes of the particles.

Fig. 3a shows the EDS spectrum of the BLSO:6Eu<sup>3+</sup> phosphor, which established the presence of Ba, La, Eu, Si, and O elements. The EDS spectrum exhibited that the majority of the Ba, La, and Eu ions occupied the L shell at 4.465, 4.650, and 5.845 keV, respectively, and small amounts of those elements occupied the M-shell at 0.8, 0.85 and 1.13 keV, respectively, in the BLSO host lattice. While, Si and O occupied their K shells at 1.74 and 0.53 keV, respectively. Fig. 3b-e show the positive ions such as Ba, La, Eu, and Si color mappings. In contrast, Fig. 3f shows the negative ion such as O mapping. As shown in Fig. 3c and 3d, it is clear that the Eu<sup>3+</sup> ions are homogeneously distributed on the La<sup>3+</sup> sites, and the layered image also exhibited the uniform distribution of Eu<sup>3+</sup> ions on the BLSO host lattice. The uniform distribution on the La<sup>3+</sup> sites in the BLSO host lattice is expected to provide efficient luminescence properties.

The inset of Fig. 3a shows the FTIR spectrum of the BLSO:6Eu<sup>3+</sup> phosphor after annealing at 1400 °C. The phosphor exhibited the IR absorption bands due to SiO<sub>4</sub> units, which can be assigned based on four types of modes such as symmetric stretching ( $\nu_1$ ), symmetric bending ( $\nu_2$ ), anti-symmetric stretching ( $\nu_3$ ), and anti-symmetric bending ( $\nu_4$ ).<sup>36,37</sup> It is evident that, from the FTIR spectrum, the stretching vibrations of  $\nu_1$  and  $\nu_3$  exhibited the intense and broad absorption bands with the band maxima at 899 and 969 cm<sup>-1</sup>, respectively, while other kinds of bending vibrations of  $\nu_2$  and  $\nu_3$  were observed at 496 and 538 cm<sup>-1</sup>, respectively. These results are in good agreement with the reported literature about the IR absorptions of SiO<sub>4</sub> units in the oxyapatite structure.<sup>34</sup> The vibrational modes of Ba, La and Eu ions are impossible to find out using the FTIR technique.

Fig. 4 shows the PLE spectra of BL<sub>(1-x)</sub>SO<sub>x</sub>:xEu<sup>3+</sup> ( $x = 1$  to 8 mol%) phosphors by monitoring the emission wavelength at



**Fig. 3** (a) EDS spectrum of the BLSO:6Eu<sup>3+</sup> phosphor. (b–g) Elemental mappings based on the EDS spectrum of the BLSO:6Eu<sup>3+</sup> phosphor (the inset of (a)(i) shows the FTIR spectrum of the BLSO:6Eu<sup>3+</sup> phosphor).

613 nm. The PLE spectra exhibited a broad band excitation between the wavelengths of 240 and 350 nm with band maxima between 283 and 288 nm, also so-called the charge transfer band (CTB). Generally, Eu<sup>3+</sup> ions doped host lattices exhibit the CTB due to the charge (electron) transfer from the completely filled 2p orbital of O<sup>2-</sup> ions to the partially filled 4f orbital of Eu<sup>3+</sup> ions,<sup>38</sup> and the CTB position varies based on the host matrix.<sup>39</sup> Besides the CTB, the BLSO:Eu<sup>3+</sup> phosphors displayed their narrow and characteristic excitation bands in the NUV region due to the intra-configurational f-f transitions of Eu<sup>3+</sup> ions, which are assigned to the electronic transitions from the <sup>7</sup>F<sub>0</sub> ground state to <sup>5</sup>D<sub>4</sub> at 363 nm, <sup>5</sup>G<sub>2</sub> at 382 nm, <sup>5</sup>L<sub>6</sub> at 394 nm, <sup>5</sup>D<sub>3</sub> at 414 nm, <sup>5</sup>D<sub>2</sub> at 464 nm, and <sup>5</sup>D<sub>1</sub> at 533 nm.

It should be noted that, from Fig. 4, the intensity of <sup>7</sup>F<sub>0</sub> → <sup>5</sup>L<sub>6</sub> transition at 394 nm is 1/4th less than the CTB intensity when 1 mol% Eu<sup>3+</sup> ions were doped into the BLSO host lattice. The intensity of <sup>7</sup>F<sub>0</sub> → <sup>5</sup>L<sub>6</sub> transition increased with increasing the

Eu<sup>3+</sup> ion concentration, and reached its maximum value at 6 mol% of Eu<sup>3+</sup> ion concentration. Here, the intensity of <sup>7</sup>F<sub>0</sub> → <sup>5</sup>L<sub>6</sub> transition is three times higher than that of CTB. The reason for the intensity variation between the CTB and <sup>7</sup>F<sub>0</sub> → <sup>5</sup>L<sub>6</sub> transition has been explained according to the crystal structure of the BLSO host lattice. The BLSO host lattice belongs to the family of oxyapatite M<sub>4</sub>RE<sub>6</sub>O(SiO<sub>4</sub>)<sub>6</sub> hexagonal structure with a space group *P6<sub>3</sub>/m*.<sup>40,41</sup> It is well known that the oxyapatite host lattice consists of the 9-fold coordinated 4f sites and 7-fold coordinated 6h sites with *C*<sub>3</sub> and *C*<sub>s</sub> point symmetry, respectively.<sup>27</sup> Ba<sup>2+</sup> and La<sup>3+</sup> ions are randomly distributed in the *C*<sub>3</sub> point symmetry of the 4f site and La<sup>3+</sup> ions are completely occupied in the *C*<sub>s</sub> point symmetry of 6h sites. According to Kubota *et al.*,<sup>42</sup> Ba<sup>2+</sup> ions occupy only the 4f sites due to the larger ionic radii as compared to the Sr<sup>2+</sup> and La<sup>3+</sup> ions (Sr<sup>2+</sup> ions occupy both 4f and 6h sites in the Sr based apatite compound). However, the Rietveld refinement results of BLSO and BLSO:6Eu<sup>3+</sup> indicate that

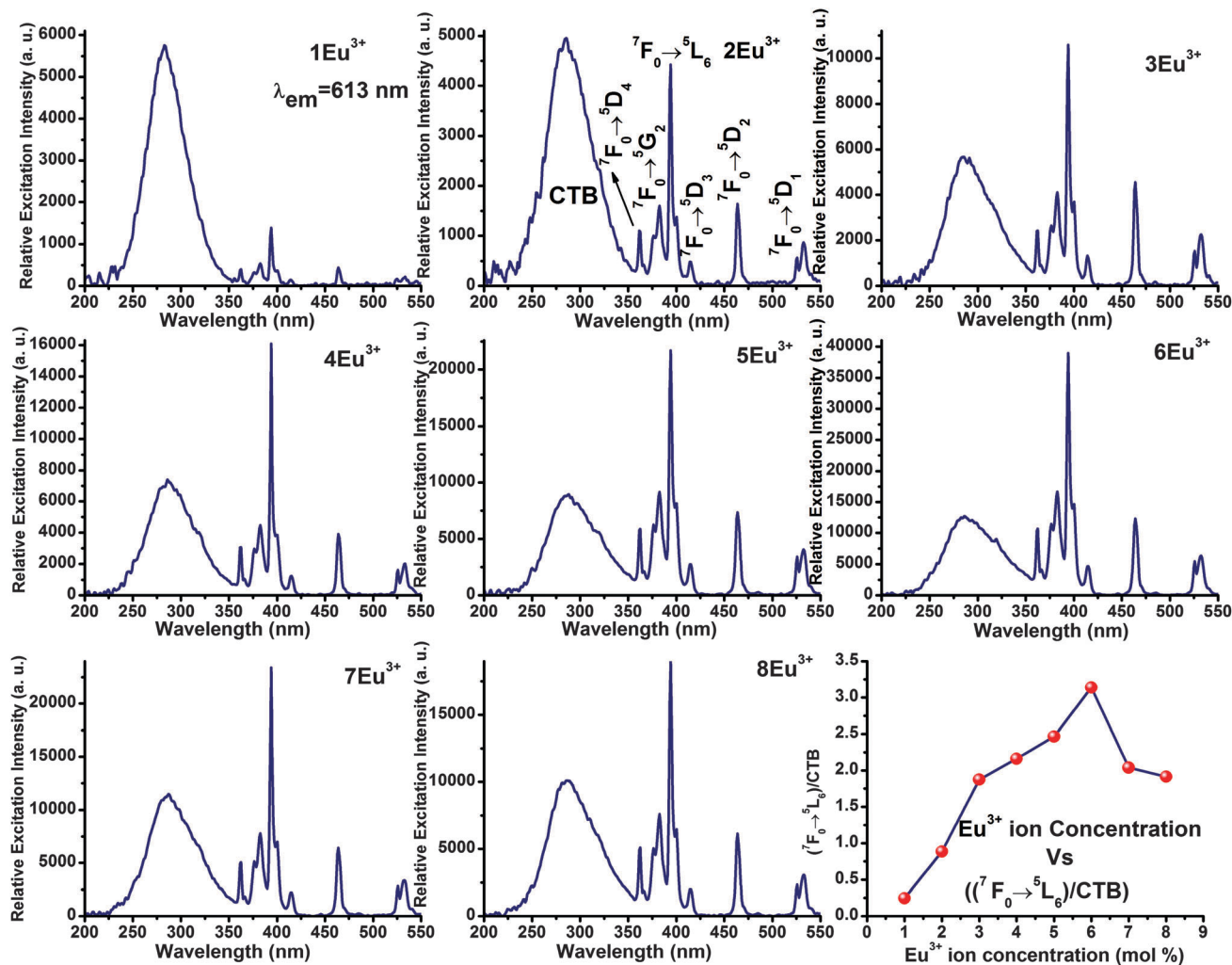


Fig. 4 PLE spectra and intensity ratio ( $(^7F_0 \rightarrow {}^5L_6)/CTB$ ) of BLSO:Eu<sup>3+</sup> phosphors as a function of Eu<sup>3+</sup> ion concentration.

the Ba<sup>2+</sup> ions occupy both 4f and 6h sites (data presented in Table 1). As analogy to the Kubota *et al.*,<sup>42</sup> who reported Sr<sub>3</sub>La<sub>6</sub>(SiO<sub>4</sub>)<sub>6</sub>:Eu<sup>3+</sup> phosphors, the Eu<sup>3+</sup> ions occupy both 4f and 6h sites similar to La<sup>3+</sup> ions because of the almost similar ionic radii, and the Eu<sup>3+</sup> ions doped into La<sup>3+</sup> sites. From ref. 42, it could be assumed that the Eu<sup>3+</sup> ions feasibly occupy the 6h sites as compared to 4f sites when the concentration of Eu<sup>3+</sup> ions increases. From Table 1, it is clear that the total site occupancy of BLSO:6Eu<sup>3+</sup> is higher than that of BLSO phosphors on the 4f site and lower on the 6h site. This result may cause the increased defects in 6h sites, while the defects perhaps decreased in the 4f sites.<sup>42</sup> The presence of defects in the 4f and 6h sites of the BLSO host lattice could change the intensity of CTB and ( ${}^7F_0 \rightarrow {}^5L_6$ ) transition because the distance between the Eu<sup>3+</sup> ions decreases with increasing Eu<sup>3+</sup> ion concentration. As a result, the interactions between the activator ions increase rather than the possibility of charge transfer between the Eu<sup>3+</sup> and O<sup>2-</sup> ions. Therefore, the intense ( ${}^7F_0 \rightarrow {}^5L_6$ ) transition appeared with increasing the Eu<sup>3+</sup> ion concentration. Furthermore, with increasing the Eu<sup>3+</sup> ion concentration, the CTB maxima shifted from 279 to 285 nm,

indicating the charge transfer from the strong absorption band in the available lowest energy to the forced electric dipole transition band of Eu<sup>3+</sup> ions in BLSO:Eu<sup>3+</sup> phosphors, which are in good agreement with the result by Hoefdraad *et al.*<sup>43</sup> According to the report, the CTB band position of Eu-doped oxide depends on the bond length of Eu-O and the coordination environment around Eu<sup>3+</sup> ions. From the observed results, it is interesting to note that the Eu<sup>3+</sup> ion concentration induced excitation spectral features are shown when the Eu<sup>3+</sup> ions are doped in the BLSO host lattice, exhibiting the broadened excitation regions as compared to the commercial Y<sub>2</sub>O<sub>3</sub>:Eu<sup>3+</sup> phosphors, as shown in Fig. 5. The calculated FWHM values in different excitation regions for the BLSO:6Eu<sup>3+</sup> and commercial Y<sub>2</sub>O<sub>3</sub>:Eu<sup>3+</sup> phosphors are shown in Fig. 5. The FWHM values indicated that the BLSO:6Eu<sup>3+</sup> phosphor has broader excitation regions, particularly in the UV, blue and green regions, which are highly useful for general lighting applications.

To verify the above mentioned features, we measured the 3D PL spectra in different excitation regions of 250–350 nm, 371–409 nm, and 457–470 nm in the UV, NUV and visible regions, respectively, as shown in Fig. 6. The 3D PL spectra

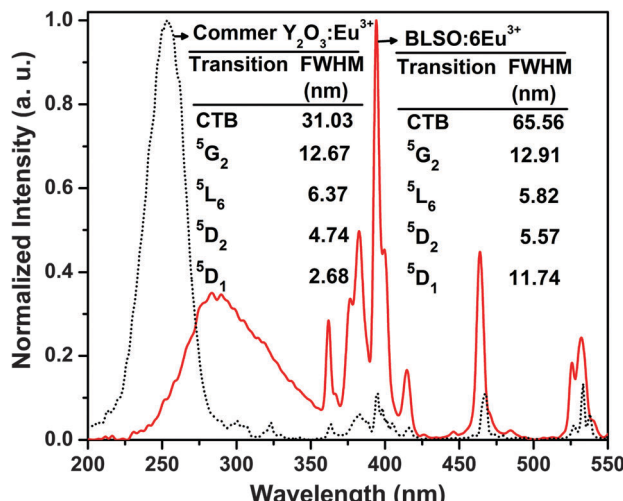


Fig. 5 Comparative PLE spectra of the commercial  $\text{Y}_2\text{O}_3:\text{Eu}^{3+}$  and BLSO:6 $\text{Eu}^{3+}$  phosphors.

were measured for every 1 nm in the selected regions. Fig. 6a(i)–c(i) show the PL intensities at each excitation wavelength and Fig. 6a(ii)–c(ii) display the contour line spectra of emitted transition intensities. All the contour line spectra exhibited the emissions from the  $^5\text{D}_0$  excited states to the  $^7\text{F}_0$ ,  $^7\text{F}_1$ ,  $^7\text{F}_2$ ,  $^7\text{F}_3$ , and  $^7\text{F}_4$  ground states. Clearly, there were no emissions from the higher energy such as  $^5\text{D}_1$  state. From the both 3D PL and contour line spectra, the strongest emission intensities were observed for the ( $^5\text{D}_0 \rightarrow ^7\text{F}_2$ ) transition, indicating that the  $\text{Eu}^{3+}$  ions occupy the low symmetry (either  $C_3$  or  $C_s$ ) sites. To compensate the red emission deficiencies for the UV, NUV and blue excitation based WLEDs, the contour line spectra support that the BLSO:Eu $^{3+}$  phosphors are promising candidates in the excitation regions between 265–320 nm, 381–385 nm, 390–400 nm, and 461–467 nm, where they provide the strongest red emission along with considerable orange emissions.

Fig. 7 shows the PL spectra of BLSO:Eu $^{3+}$  phosphors as a function of Eu $^{3+}$  ion concentration. The PL spectra exhibited a stronger emission band with a peak at 613 nm. This can be attributed to the hypersensitive forced electric-dipole  $^5\text{D}_0 \rightarrow ^7\text{F}_2$  transition of the Eu $^{3+}$  ions, which is located at the non-inversion symmetry sites. The moderate emission bands at 591, 594, and 598 nm are due to the magnetic-dipole  $^5\text{D}_0 \rightarrow ^7\text{F}_1$  transition and the other two emission bands at 579 and 586 nm are due to the  $^5\text{D}_0 \rightarrow ^7\text{F}_0$  transition of Eu $^{3+}$  ions. Note that the significant emission bands were not observed at the higher energy  $^5\text{D}_1$  and  $^5\text{D}_2$  levels in the blue and green wavelength regions. The reason is that the energy gaps between the  $^5\text{D}_2$  and  $^5\text{D}_1$  or  $^5\text{D}_1$  and  $^5\text{D}_0$  of Eu $^{3+}$  ions are smaller and, in the oxyapatite, which can be bridged by the vibration energies of the silicate groups. The higher  $^5\text{D}_2$  and  $^5\text{D}_1$  excited levels are then relaxed once to the lowest  $^5\text{D}_0$  excited level.<sup>35</sup>

Furthermore, the shapes of emission spectra at different Eu $^{3+}$  ion concentrations when annealed at 1400 °C are similar. As the Eu $^{3+}$  ion concentration increased from 1 to 6 mol%, the emission intensity also increased. However, when the concentration

of Eu $^{3+}$  ions increased above 6 mol%, the emission intensity decreased due to the concentration quenching. Similarly, the asymmetric ratio (red (R)/orange (O)) increased with increasing the concentration of Eu $^{3+}$  ions up to 6 mol%, while the asymmetric ratio decreased when the Eu $^{3+}$  ion concentration increased over 6 mol%, as can be seen in Fig. 7. The concentration quenching could occur due to the following reasons:<sup>44</sup> (i) when the activator concentration is increased, the resonance between the activator ions causes the enhancement of excitation migration, and thus the excitation energy reaches their quenching centers, or (ii) the activator ions are paired or may be coagulated and are shifted to their quenching center. Based on the observed results, the concentration of Eu $^{3+}$  ions was optimized at 6 mol%.

The lifetime measurement was performed for the optimized BLSO:6Eu $^{3+}$  phosphor at 394 nm excitation and 613 nm emission wavelengths, as shown in Fig. 8a. The decay curve was well fitted to a single exponential function of  $I(t) = I_0(t) \exp(-t/\tau)$ , where  $I(t)$  is the decaying luminescence intensity at time  $t$ ,  $I_0$  is the initial intensity and  $\tau$  is the decay time. This exponential fitting supports the study by Kubota *et al.*<sup>42</sup> and clarifies that majority of the emissions originating from one cationic site. The calculated lifetime was found to be around 1558 μs. To explore the concentration quenching mechanism, the critical distance ( $R_c$ ) between the Eu $^{3+}$  ions was calculated according to the Blasse proposed equation:<sup>45,46</sup>

$$R_c \approx 2 \left[ \frac{3V}{4\pi X_c N} \right]^{\frac{1}{3}} \quad (2)$$

where  $V$  is the volume of the unit cell,  $N$  is the cationic sites in the host lattice unit cell, and  $X_c$  is the optimized concentration of activator ions. For the BLSO host lattice,  $V = 604.95 \text{ \AA}^3$ ,  $N = 10$  and the optimum concentration of Eu $^{3+}$  ions in the BLSO host lattice is  $X_c = 0.06$ . Therefore, the  $R_c$  value was found to be about 12.44 Å. For more detailed understanding of the concentration quenching mechanism, the relationship plot between the  $\log(x)$  versus  $\log(i/x)$  for the luminescence intensity of BLSO:Eu $^{3+}$  at 613 nm when excited at the wavelength of 394 nm is shown in Fig. 8b. The luminescence intensity ( $i$ ) and the substituted mole fraction ( $x$ ) of Eu $^{3+}$  ions for the corresponding doping levels are expressed according to the Dexter's law, as follows:<sup>47</sup>

$$\log\left(\frac{i}{x}\right) = C - \left(\frac{\theta}{3}\right) \log(x) \quad (3)$$

where  $C$  is a constant, and  $\theta = 6, 8$ , and 10 corresponding to the electric dipole-dipole, dipole-quadrupole, and quadrupole-quadrupole interactions, respectively.<sup>48</sup> The experimental data of BLSO:Eu $^{3+}$  were fitted by a straight line with a slope of 2.093, and the  $\theta$  value was found to be 6.28. From the obtained results, the electric dipole-dipole interactions are responsible for the concentration quenching of Eu $^{3+}$  ions in the BLSO host lattice.

In order to explore the quality of the red emission obtained from the BLSO:6Eu $^{3+}$  phosphor, the PL spectra were compared with the commercial  $\text{Y}_2\text{O}_3:\text{Eu}^{3+}$  phosphors when excited with the wavelength of 394 nm as shown in Fig. 9. The comparative

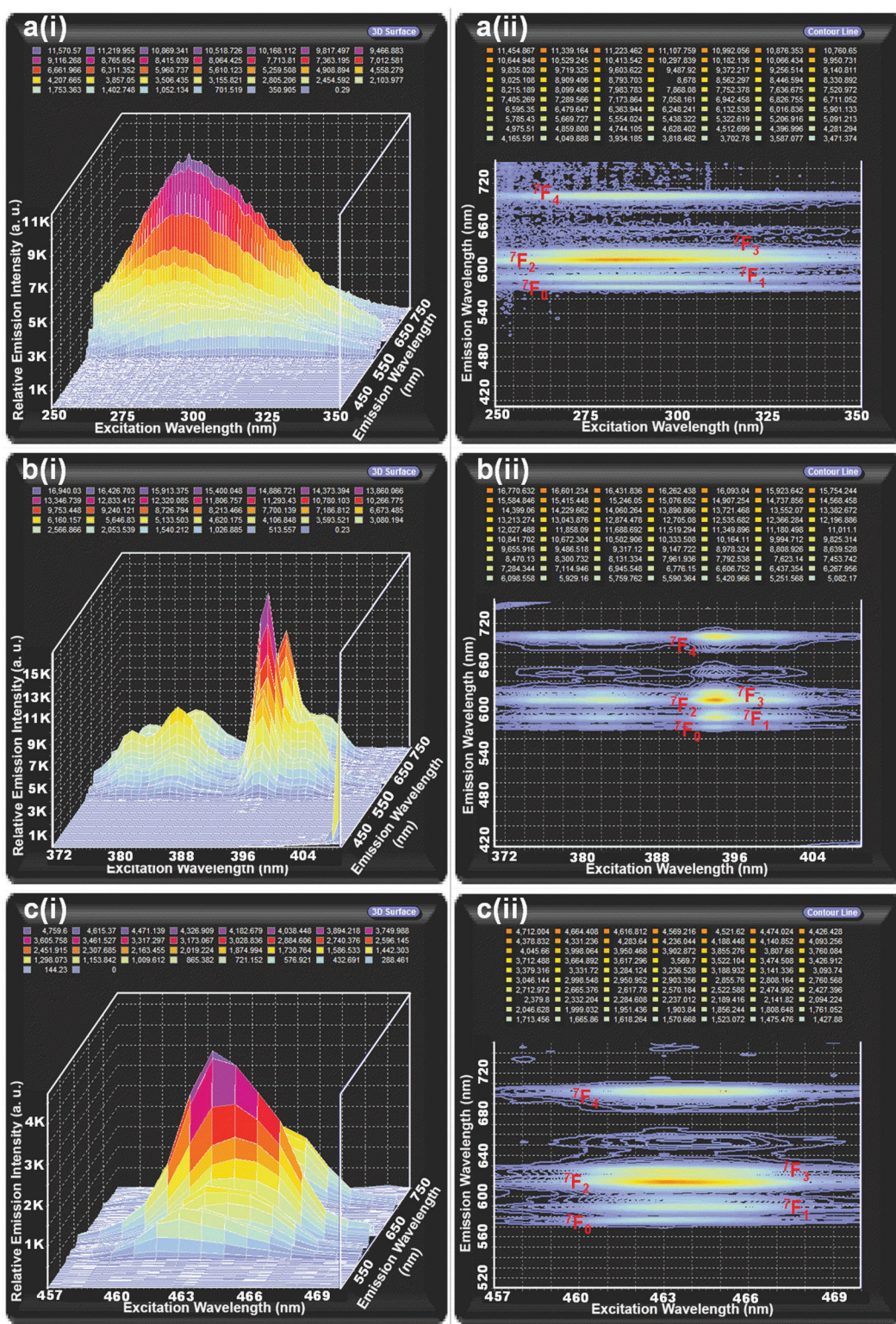


**Fig. 6** 3D PL spectra and their contour lines of the BLSO:6Eu<sup>3+</sup> phosphor as a function of excitation wavelength for the excitation regions between (a) 250–350 nm, (b) 370–410 nm and (c) 457–470 nm.

PL spectra revealed that there is a large difference between the emitting regions of the commercial and the BLSO:6Eu<sup>3+</sup> phosphor. The FWHM value of the first stark splitting (wavelength

range between 602–620 nm) of forced electric dipole transition of the BLSO:6Eu<sup>3+</sup> phosphor was 8.92 nm whereas the commercial Y<sub>2</sub>O<sub>3</sub>:Eu<sup>3+</sup> phosphor had a FWHM value of 3.02 nm,

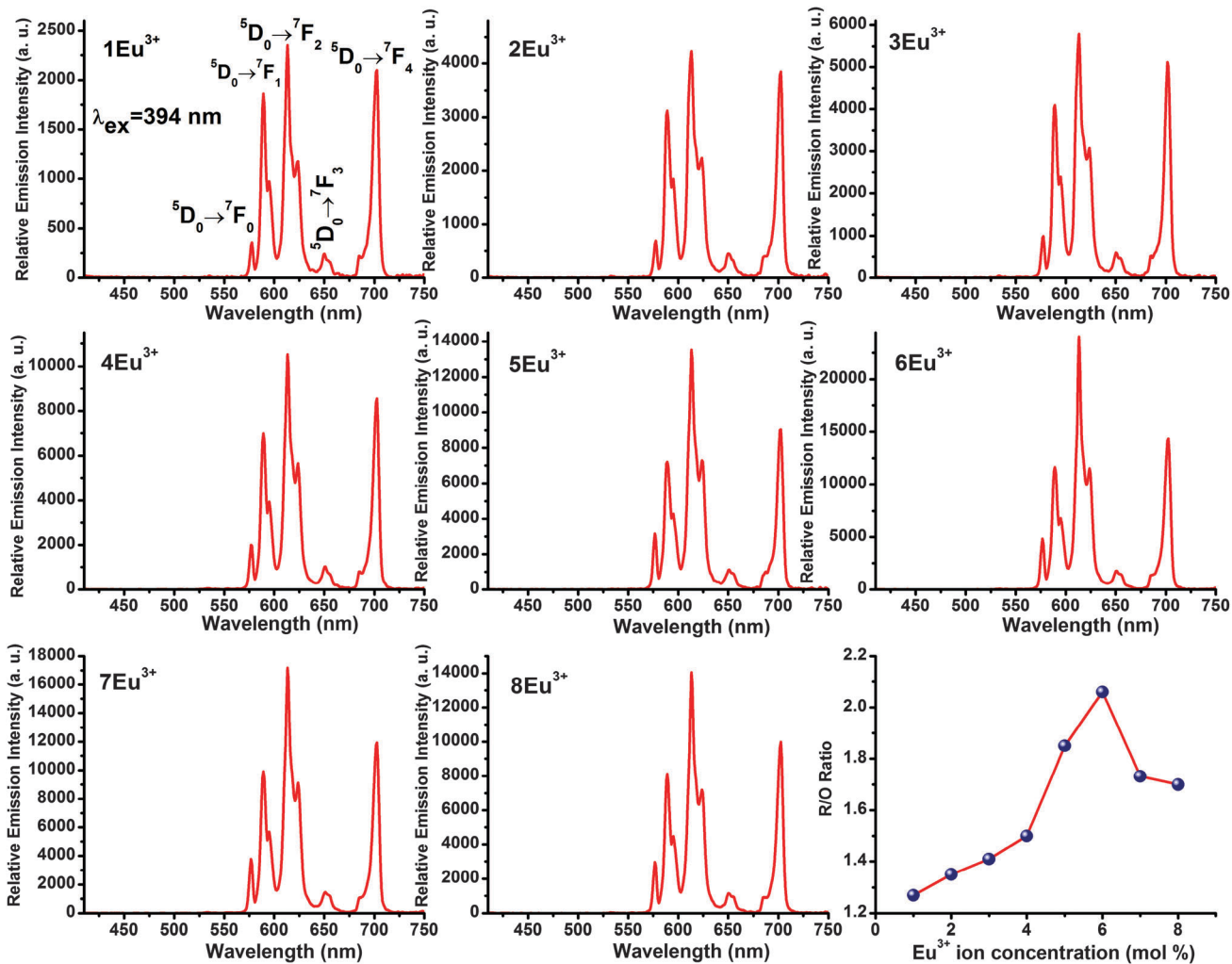


Fig. 7 PL spectra and asymmetry ratio of the BLSO:6Eu<sup>3+</sup> phosphor as a function of Eu<sup>3+</sup> ion concentration.

indicating that the BLSO:Eu<sup>3+</sup> phosphors have much broader emission than that of the commercial Y<sub>2</sub>O<sub>3</sub>:Eu<sup>3+</sup> phosphors. However, in contrast to the emission region occupancy, the asymmetric ratio of the BLSO:6Eu<sup>3+</sup> shows a lower value ( $R = 2.58$ ) than that of the commercial Y<sub>2</sub>O<sub>3</sub>:Eu<sup>3+</sup> ( $R = 8.75$ ). The decreased  $R$  value means the decreased red color purity. However, by considering the intensity of  ${}^5\text{D}_0 \rightarrow {}^7\text{F}_4$  transition, the BLSO:Eu<sup>3+</sup> phosphors provide the better red emission, which are suitable as a red compensator and offer natural white light when combined with the Y<sub>3</sub>Al<sub>5</sub>O<sub>12</sub> (YAG):Ce<sup>3+</sup> yellow phosphors because the excitation peaks of the BLSO:6Eu<sup>3+</sup> at 466 and 533 nm are overlapped well with the respective excitation and emission peaks of the YAG:Ce<sup>3+</sup> phosphors. This type of phosphor-converted WLED could contribute to high CRI display systems and this warm white light is also useful to create a decent atmosphere in the indoors. Moreover, it is also possible to obtain the deep red emission when using the suitable cut-off filters. This deep red emission is useful for cultivation.

The temperature-dependent PL properties are important for testing the suitability of phosphors for their applications in the

development of WLEDs because the thermal quenching property is one of the crucial technological parameters.<sup>49,50</sup> The junction temperature of LEDs is nearly about 120 °C and above that temperature, significant thermal quenching as well as shifting of emission color is possible.<sup>51</sup> Earlier reports suggested that the LED phosphors should endure at elevated temperatures (more than 150 °C), with all the associated consequences such as chemical, physical and thermal stabilities.<sup>52</sup> Thus, we performed the temperature dependent measurements in the temperature range of 27–177 °C for the BLSO:6Eu<sup>3+</sup> phosphor. Fig. 10 shows the temperature dependent relative emission intensities of the BLSO:6Eu<sup>3+</sup> phosphor by exciting with the wavelengths of 394 nm at an interval of 10 °C. Because of the thermal quenching, the emission intensity dropped by ~37 and 64% at 120 and 177 °C, respectively. However, deep analysis is required for the available defects in the low symmetry sites and distribution of Eu<sup>3+</sup> ions in the BLSO host lattice.

Moreover, the absolute quantum yield ( $\eta$ ) and the absorption efficiency ( $\alpha_{\text{abs}}$ ) of the BLSO:6Eu<sup>3+</sup> phosphor were established

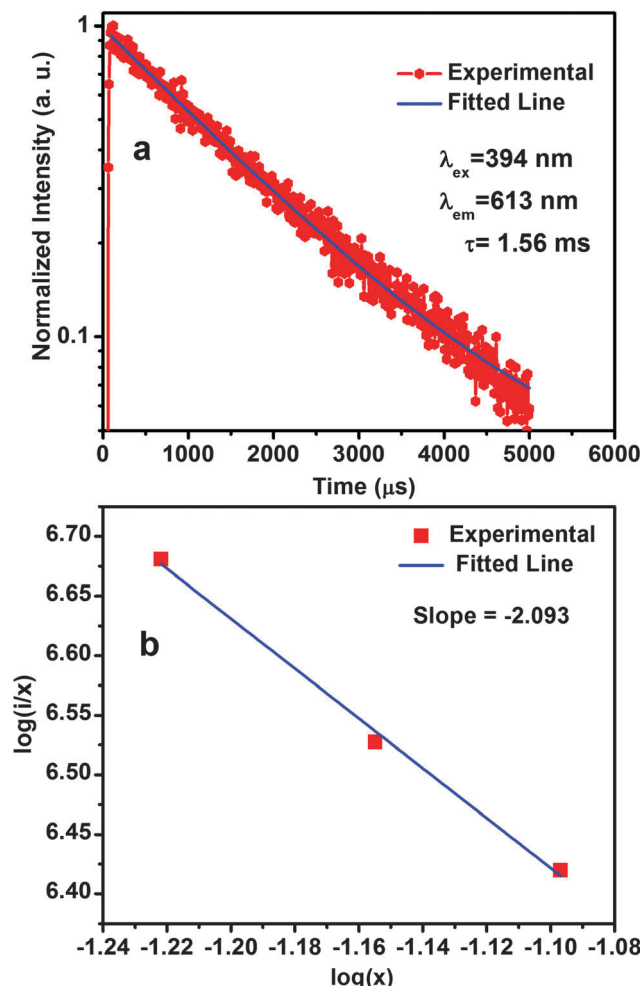


Fig. 8 (a) Decay curve of the BLSO:6Eu<sup>3+</sup> phosphor and (b) relationship plot between log(x) and log(I/x) for 613 nm emission under the excitation of 394 nm.

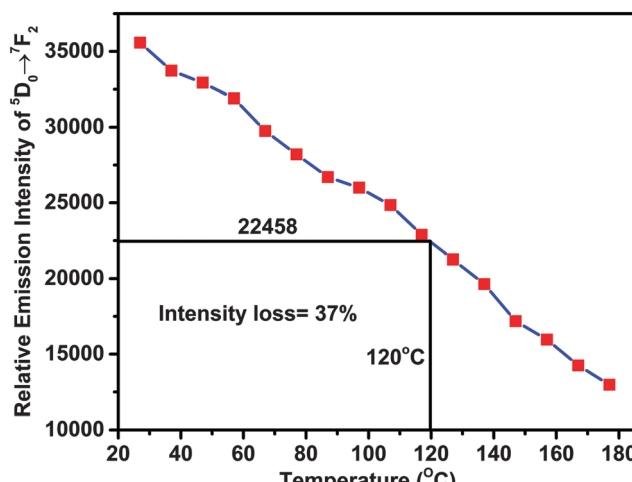


Fig. 10 Temperature-dependent PL emission intensities of the BLSO:6Eu<sup>3+</sup> phosphor.

based on the integrating sphere method using the following equations:<sup>53</sup>

$$\eta = \frac{\int \lambda \cdot P(\lambda) d\lambda}{\int \lambda \{E(\lambda) - R(\lambda)\} d\lambda} \quad (4)$$

$$\alpha_{abs} = \frac{\int \{E(\lambda) - R(\lambda)\} d\lambda}{\int \lambda \cdot E(\lambda) d\lambda} \quad (5)$$

Here,  $E(\lambda)$ ,  $R(\lambda)$ , and  $P(\lambda)$  are the number of photons in the spectrum of excitation, reflectance and emission of the phosphors, respectively. For the current synthesis conditions, the  $\eta$  and  $\alpha_{abs}$  values are 65 and 30%, respectively, at an excitation wavelength of 394 nm. It is also a noticeable fact that the  $\eta$  value of the commercial Y<sub>2</sub>O<sub>3</sub>:Eu<sup>3+</sup> under 394 nm excitation is only 9.6%,<sup>54</sup> which is almost 7 times lower than that of the BLSO:6Eu<sup>3+</sup> phosphor.

In continuation to the PL measurements, the CL properties of BLSO:Eu<sup>3+</sup> phosphors as a function of accelerating voltage and filament current were studied to explore their potentiality for the efficient red region in FED systems. Fig. 11a shows the low electron beam excitation (accelerating voltage = 5 kV and filament current = 55 μA) based CL spectra of the BLSO:6Eu<sup>3+</sup> and the commercial Y<sub>2</sub>O<sub>3</sub>:Eu<sup>3+</sup> phosphors. The CL spectrum of BLSO:6Eu<sup>3+</sup> exhibited similar features to the PL spectrum. However, the commercial phosphor shows slightly different behavior from the PL spectrum. Under low electron beam excitation, as compared to the BLSO:6Eu<sup>3+</sup> phosphor, the commercial Y<sub>2</sub>O<sub>3</sub>:Eu<sup>3+</sup> phosphors showed higher intensity, but considerable emission bands appeared in the higher energy ( ${}^5D_1$  and  ${}^5D_2$  regions) regions, indicating that the red emission purity is not stable for the commercial phosphor, which depends upon the source of excitation. However, without depending on the excitation source, the BLSO:Eu<sup>3+</sup> phosphors exhibited a stable emission spectrum, which is the better advantage for obtaining the similar color parameters when using different excitation sources. Furthermore, Fig. 11b and c show the CL intensities of the BLSO:6Eu<sup>3+</sup> phosphor as

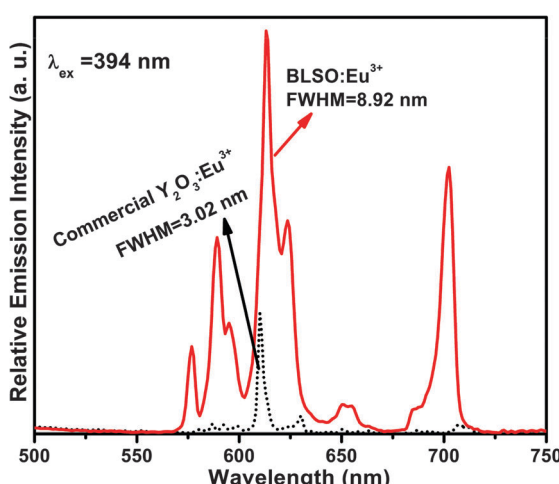


Fig. 9 Comparative PL spectra of the commercial Y<sub>2</sub>O<sub>3</sub>:Eu<sup>3+</sup> and BLSO:Eu<sup>3+</sup> phosphor under an excitation of 394 nm.

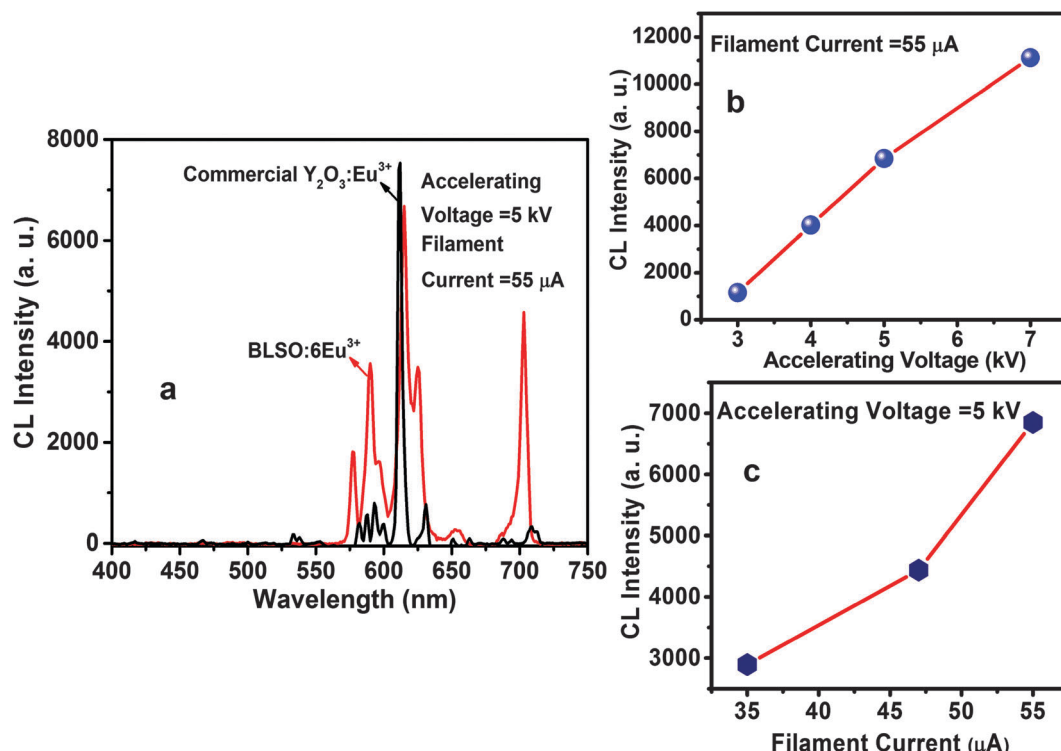


Fig. 11 (a) CL spectra of the BLSO:6Eu<sup>3+</sup> and commercial Y<sub>2</sub>O<sub>3</sub>:Eu<sup>3+</sup> phosphors. Comparative CL intensity as a function of (b) accelerating voltage and (c) filament current.

a function of accelerating voltage and filament current. It was observed that the CL intensity of the BLSO:6Eu<sup>3+</sup> phosphor increased as the accelerating voltage increased from 3 to 7 kV at a fixed filament current of 55 μA and no optimization was observed up to our measured conditions, as can be seen in Fig. 11b. A similar behavior was observed for the BLSO:6Eu<sup>3+</sup> phosphor when increasing the filament current from 35 to 55 μA under a fixed accelerating voltage of 5 kV, as shown in Fig. 11c. The reason because more plasma will be generated thanks to the deeper electron penetration depth by the recombination of more excitons (electron–hole pairs) when increasing the filament current or accelerating voltage resulted in more Eu<sup>3+</sup> ions being excited from the boundary or surface including the inside of particles. The electron penetration depth for the BLSO:6Eu<sup>3+</sup> phosphor was estimated by the following empirical formula:<sup>44</sup>

$$L [\text{\AA}] = 250 \left( \frac{A}{\rho} \right) \left( \frac{E}{Z^2} \right)^n n = \frac{1.2}{1 - 0.29 \log Z} \quad (6)$$

Here,  $A$  is the atomic or molecular weight of the compound,  $\rho$  is the bulk density (for BLSO,  $\rho = 3.5 \text{ g cm}^{-3}$ ) of the material,  $E$  is the accelerating voltage, and  $Z$  is the atomic number per molecule. For the BLSO:6Eu<sup>3+</sup> phosphor,  $A = 1997.57$ , and  $Z = 869.26$ , the calculated penetration depths were  $8 \times 10^{-4}$ ,  $8.4 \times 10^{-3}$ ,  $5 \times 10^{-2}$  and  $0.79 \text{ \AA}$  at the accelerating voltages of 3, 4, 5, and 7 kV, respectively.

The Commission International de l'Eclairage (CIE) chromaticity coordinates of the BLSO:6Eu<sup>3+</sup> and commercial Y<sub>2</sub>O<sub>3</sub>:Eu<sup>3+</sup>

phosphors were calculated for the PL spectra when excited with the wavelength of 394 nm and for the CL spectra at an accelerating voltage of 5 kV and a filament current of 55 μA. Under 394 nm excitation, the CIE chromaticity coordinates of the Y<sub>2</sub>O<sub>3</sub>:Eu<sup>3+</sup> phosphors were (0.654, 0.344), while the coordinates were (0.634, 0.365) for the BLSO:6Eu<sup>3+</sup> phosphor, as shown in Fig. 12. As compared

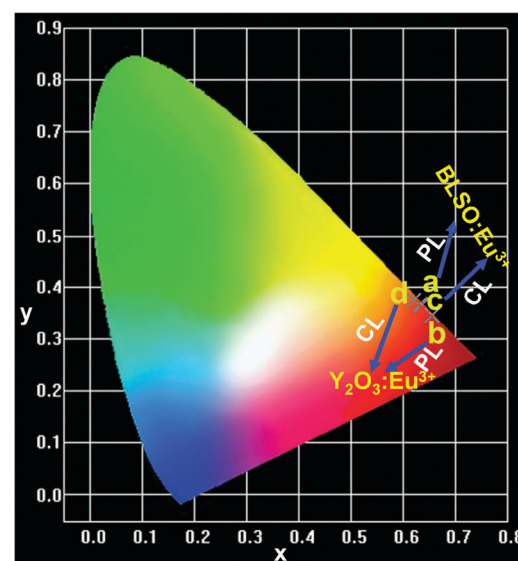


Fig. 12 CIE chromaticity coordinates of the commercial Y<sub>2</sub>O<sub>3</sub>:Eu<sup>3+</sup> and BLSO:6Eu<sup>3+</sup> phosphors: from PL (a) (0.634, 0.365), (b) (0.654, 0.344), and from CL (c) (0.632, 0.368) and (d) (0.621, 0.375).

to the BLSO:6Eu<sup>3+</sup> phosphor, the commercial Y<sub>2</sub>O<sub>3</sub>:Eu<sup>3+</sup> phosphor had a higher red color purity under 394 nm excitation. However, by considering the CIE chromaticity coordinates of CL spectra, it is clear that the color purity of Y<sub>2</sub>O<sub>3</sub>:Eu<sup>3+</sup> (0.621, 0.375) decreases due to the presence of higher <sup>5</sup>D<sub>J</sub> levels of Eu<sup>3+</sup> ions, while the color coordinates of the BLSO:6Eu<sup>3+</sup> phosphor vary slightly, which may be the experimental errors and are negligible. The appearance of higher <sup>5</sup>D<sub>J</sub> levels is due to the deeper penetration depth. From the CIE chromaticity of both the PL and CL spectra, the BLSO:Eu<sup>3+</sup> phosphors show the stable color parameters than that of the commercial Y<sub>2</sub>O<sub>3</sub>:Eu<sup>3+</sup> phosphors, which is useful for fabricating the artificial white light to be similar to those of natural white light because of its better spectral overlap.<sup>55,56</sup>

## Conclusions

The BLSO:Eu<sup>3+</sup> phosphors were successfully synthesized by a modified citrate sol-gel process. The XRD patterns confirmed their oxyapatite structure with the space group of *P6<sub>3</sub>/m* after being annealed at 1400 °C. The FTIR spectrum exhibited the presence of SiO<sub>4</sub> units in the oxyapatite structure and the SEM image showed the irregular morphology of BLSO:Eu<sup>3+</sup> particles. The EDS elemental mapping revealed that the Eu<sup>3+</sup> ions were distributed homogeneously on the La<sup>3+</sup> sites. The PLE spectra of BLSO:Eu<sup>3+</sup> phosphors exhibited the strong absorption in the NUV region due to the presence of defects in the 4f and 6h sites of the BLSO host lattice. The PL spectra displayed intense red emission (<sup>5</sup>D<sub>0</sub> → <sup>7</sup>F<sub>2</sub>) along with considerable orange (<sup>5</sup>D<sub>0</sub> → <sup>7</sup>F<sub>1</sub>) and deep red (<sup>5</sup>D<sub>0</sub> → <sup>7</sup>F<sub>2</sub>) emissions and exhibited better emission properties with better FWHM values compared to the commercial Y<sub>2</sub>O<sub>3</sub>:Eu<sup>3+</sup> phosphors. The 3D PL spectra revealed their strong emission characteristics under UV, NUV and visible excitation regions. This perception provides the hint of their suitability in the development of UV, NUV and visible excitations based on lighting and display systems. The CL properties confirmed that the BLSO:Eu<sup>3+</sup> phosphors emit relatively stable red emissions under different excitation sources as compared to those of the commercial Y<sub>2</sub>O<sub>3</sub>:Eu<sup>3+</sup> phosphors. The increased CL intensity of BLSO:Eu<sup>3+</sup> phosphors with increasing the accelerating voltage and filament current indicates the possibility of their promising applications in the development of FED systems.

## Acknowledgements

This work was supported by the National Research Foundation of Korea (NRF) Grant funded by the Korea Government (MSIP) (No. 2015R1A5A1037656).

## References

- T. Bright, *Scientific Background on the Nobel Prize in Physics*, The Royal Swedish Academy of Sciences, 2014.
- E. Pavitra, G. S. R. Raju, J. Y. Park, L. Wang, B. K. Moon and J. S. Yu, *Sci. Rep.*, 2015, **5**, 10296.
- F. Kang, Y. Zhang, L. Wondraczek, J. Zhu, X. Yang and M. Peng, *J. Mater. Chem. C*, 2014, **2**, 9850–9857.
- F. Kang, Y. Zhang and M. Peng, *Inorg. Chem.*, 2015, **54**, 1462–1473.
- H. He, Y. Zhang, Q. Pan, G. Wu, G. Dong and J. Qiu, *J. Mater. Chem. C*, 2015, **3**, 5419–5429.
- M. Zhang, Y. Liang, R. Tang, D. Yu, M. Tong, Q. Wang, Y. Zhu, X. Wu and G. Li, *RSC Adv.*, 2014, **4**, 40626–40637.
- H. A. Höppe, *Angew. Chem., Int. Ed.*, 2009, **48**, 3572–3582.
- S. Miao, Z. Xia, M. S. Molokeev, M. Chen, J. Zhang and Q. Liu, *J. Mater. Chem. C*, 2015, **3**, 4616–4622.
- J. Zhang, Y. He, Z. Qiu, W. Zhang, W. Zhou, L. Yu and S. Lian, *Dalton Trans.*, 2014, **43**, 18134–18145.
- R. Boonsin, G. Chadeyron, J.-P. Roblin, D. Boyer and R. Mahiou, *J. Mater. Chem. C*, 2015, **3**, 9580–9587.
- J. Dwivedi, P. Kumar, A. Kumar, Sudama, V. N. Singh, B. P. Singh, S. K. Dhawan, V. Shanker and B. K. Gupta, *RSC Adv.*, 2014, **4**, 54936–54947.
- M. Shang, C. Li and J. Lin, *Chem. Soc. Rev.*, 2014, **43**, 1372–1386.
- D. A. Steigerwald, J. C. Bhat, D. Collins, R. M. Fletcher, M. O. Holcomb, M. J. Ludowise, P. S. Martin and S. L. Rudaz, *IEEE J. Sel. Top. Quantum Electron.*, 2002, **8**, 310–320.
- S.-P. Kuang, Y. Meng, J. Liu, Z.-C. Wu and L.-S. Zhao, *Optik*, 2013, **124**, 5517–5519.
- J. K. Sheu, S. J. Chang, C. H. Kuo, Y. K. Su, L. W. Wu, Y. C. Lin, W. C. Lai, J. M. Tsai, G. C. Chi and R. K. Wu, *IEEE Photonics Technol. Lett.*, 2003, **15**, 18–20.
- Z. Hao, J. Zhang, X. Zhang, X. Sun, Y. Luo, S. Lu and X.-j. Wang, *Appl. Phys. Lett.*, 2007, **90**, 261113.
- Z. Xia, J. Zhuang, H. Liu and L. Liao, *J. Phys. D: Appl. Phys.*, 2012, **45**, 015302.
- W. Lü, Z. Hao, X. Zhang, X. Wang and J. Zhang, *Opt. Mater.*, 2011, **34**, 261–264.
- Z. Xia, J. Zhuang, A. Meijerink and X. Jing, *Dalton Trans.*, 2013, **42**, 6327–6336.
- W. Lü, W. Lv, Q. Zhao, M. Jiao, B. Shao and H. You, *Inorg. Chem.*, 2014, **53**, 11985–11990.
- G. Tamulaitis, P. Duchovskis, Z. Bliznikas, K. Breive, R. Ulinskaitė, A. Brazaitytė, A. Novičkovas and A. Žukauskas, *J. Phys. D: Appl. Phys.*, 2005, **38**, 3182.
- P. S. C. Schulze, L. A. Barreira, H. G. C. Pereira, J. A. Perales and J. C. S. Varela, *Trends Biotechnol.*, 2014, **32**, 422–430.
- O. A. Lipina, L. L. Surat, A. P. Tyutyunnik, I. I. Leonidov, E. G. Vovkotrub and V. G. Zubkov, *CrystEngComm*, 2015, **17**, 3333–3344.
- M. S. Wickleder, *Chem. Rev.*, 2002, **102**, 2011–2088.
- I. P. Sahu, D. P. Bisen and N. Brahme, *J. Radiat. Res. Appl. Sci.*, 2015, **8**, 381–388.
- K. Li, J. Fan, M. Shang, H. Lian and J. Lin, *J. Mater. Chem. C*, 2015, **3**, 9989–9998.
- M. Wierzbicka-Wieczorek, M. Göckeritz, U. Kolitsch, C. Lenz and G. Giester, *Eur. J. Inorg. Chem.*, 2015, 948–963.
- J. Lin and Q. Su, *Mater. Chem. Phys.*, 1994, **38**, 98–101.
- J. Lin and S. Su, *J. Alloys Compd.*, 1994, **210**, 159–163.
- G. Li, D. Geng, M. Shang, C. Peng, Z. Cheng and J. Lin, *J. Mater. Chem.*, 2011, **21**, 13334–13344.

- 31 Z. Sun, M. Wang, X. Song and Z. Jiang, *J. Rare Earths*, 2013, **31**, 957–961.
- 32 Y. Liu, Z. Wang, J. Zhong, F. Pan, H. Liang and Z. Xiao, *Mater. Lett.*, 2014, **129**, 130–133.
- 33 J. Sokolnicki and E. Zych, *J. Lumin.*, 2015, **158**, 65–69.
- 34 M. G. Zuev, A. M. Arpov and A. S. Shkvarin, *J. Solid State Chem.*, 2011, **184**, 52–58.
- 35 G. Seeta Rama Raju, H. C. Jung, J. Y. Park, B. K. Moon, R. Balakrishnaiah, J. H. Jeong and J. H. Kim, *Sens. Actuators, B*, 2010, **146**, 395–402.
- 36 R. El Ouenzerfi, C. Goutaudier, G. Panczer, B. Moine, M. T. Cohen-Adad, M. Trabelsi-Ayedi and N. Kbir-Ariguib, *Solid State Ionics*, 2003, **156**, 209–222.
- 37 G. S. R. Raju, Y. H. Ko, E. Pavitra, J. S. Yu, J. Y. Park, H. C. Jung and B. K. Moon, *Cryst. Growth Des.*, 2012, **12**, 960–969.
- 38 M. Jiao, N. Guo, W. Lu, Y. Jia, W. Lv, Q. Zhao, B. Shao and H. You, *Dalton Trans.*, 2013, **42**, 12395–12402.
- 39 A. K. Singh, S. K. Singh and S. B. Rai, *RSC Adv.*, 2014, **4**, 27039–27061.
- 40 Y. Wen, Y. Wang, F. Zhang and B. Liu, *Mater. Chem. Phys.*, 2011, **129**, 1171–1175.
- 41 G. Li, Y. Zhang, D. Geng, M. Shang, C. Peng, Z. Cheng and J. Lin, *ACS Appl. Mater. Interfaces*, 2012, **4**, 296–305.
- 42 S. Kubota, R. L. Stanger, Y. Suzuyama, H. Yamane and M. Shimada, *J. Electrochem. Soc.*, 2002, **149**, H134–H137.
- 43 H. E. Hoefdraad, F. M. A. Stegers and G. Blasse, *Chem. Phys. Lett.*, 1975, **32**, 216–217.
- 44 W. M. Yen and H. Yamamoto, *Phosphor handbook*, CRC Press, 2006.
- 45 G. Blasse, *Philips Res. Rep.*, 1969, **24**, 131–144.
- 46 Y.-C. Chang, C.-H. Liang, S.-A. Yan and Y.-S. Chang, *J. Phys. Chem. C*, 2010, **114**, 3645–3652.
- 47 D. L. Dexter, *J. Chem. Phys.*, 1953, **21**, 836–850.
- 48 L. G. Van Uitert, E. F. Dearborn and J. J. Rubin, *J. Chem. Phys.*, 1967, **47**, 547–553.
- 49 J. H. Ryu, Y.-G. Park, H. S. Won, S. H. Kim, H. Suzuki, J. M. Lee, C. Yoon, M. Nazarov, D. Y. Noh and B. Tsukerblat, *J. Electrochem. Soc.*, 2008, **155**, J99–J104.
- 50 R. Zhu, Y. Huang and H. J. Seo, *J. Am. Ceram. Soc.*, 2011, **94**, 3380–3385.
- 51 M. Arik, C. Becker, S. Weaver and J. Petroski, *Proc. SPIE*, 2004, **5187**, 64–75.
- 52 C. Feldmann, T. Jüstel, C. R. Ronda and P. J. Schmidt, *Adv. Funct. Mater.*, 2003, **13**, 511–516.
- 53 K. Ohkubo and T. Shigeta, *J. Illum. Eng. Inst. Jpn*, 1999, **83**, 87–93.
- 54 S. Long, J. Hou, G. Zhang, F. Huang and Y. Zeng, *Ceram. Int.*, 2013, **39**, 6013–6017.
- 55 L. S. Kumari, P. P. Rao, M. Thomas and P. Koshy, *J. Electrochem. Soc.*, 2009, **156**, P127–P131.
- 56 S. Fujihara and K. Tokumo, *Chem. Mater.*, 2005, **17**, 5587–5593.